EVALUATION OF GRID-FORMING CONVERTER'S IMPACT ON DISTANCE PROTECTION PERFORMANCE

Di Liu[1], Qiteng Hong[1*], Md Asif Uddin Khan[1], Adam Dyśko[1], Agusti Egea Alvarez[1] and Campbell Booth[1]

[1]Department of Electronic and Electrical Engineering, University of Strathclyde, Glasgow, United Kingdom
**q.hong@strath.ac.uk*

Keywords: DISTANCE PROTECTION, GRID-FORMING CONVERTER, CURRENT LIMITATION, FAULT-RIDE THROUGH, REAL-TIME DIGITAL SIMULATION

Abstract

Motivated by the net-zero carbon emission target, the GB transmission system has seen a massive increase in the amount of Converter Based Resources (CBRs). Grid-Forming Converters (GFMs) have attracted significant interests for supporting the future system operability with high penetration of renewables due to their various more desirable properties compared with Grid-Following Converters (GFLs), e.g., stronger capability to operate in weak grids. Recent research work has found that Fault-Ride Through (FRT) strategies of CBRs have significant impact on the distance protection performance, and comprised protection operation was observed when synchronous generation sources were replaced with CBRs. However, existing research work has mainly focused on the impact of the GFLs' FRT on distance protection, while the impact of GFMs, which could have very different FRT strategies, has not been comprehensively investigated. In this paper, a GFM with two typically used FRT implementations, i.e., the current control based FRT and the virtual impedance based FRT, is developed in the Real-Time Digital Simulator (RTDS) and the impact of the two FRT methods on distance protection is investigated for both balanced and unbalanced fault conditions. By comparing the relay performance with two FRT strategies, it is found that the distance protection appears to have better performance in terms of faulty phase selection, accurate impedance measurement and impedance measurement stability when the virtual impedance-based FRT is adopted by the GFM.

1 Introduction

In recent years, massive amounts of Converter Based Resources (CBRs), e.g., renewable generation and HVDC systems, have been integrated to the power systems worldwide with an aim to achieve the net-zero carbon emission targets [1] and this trend is expected to continue in the coming decades. Presently, vast majority of the connected CBRs operate in the grid-following mode to regulate the power and voltage in the network by governing the injected currents [2]. For Grid-Following Converters (GFLs), the Phase-Locked-Loops (PLLs) are typically used to estimate the angle of the voltage phasors at the Point of Common Coupling (PCC) and thus to synchronise with the AC network [3]. As a result, the performance of GFLs is highly dependent on the strength of the connected network and GFLs could start experiencing operational issues, e.g. loss of synchronisation [3][4], resonant problems [5] and limited active power transfer [6], in weak systems, e.g., when Short Circuit Ratio (SCR) < 3 [7].

To improve the converter performance in weak systems and to enable the grid forming capability in islanded systems, grid-forming control has been proposed [9], which, unlike the GFLs, can synchronise to the main network by controlling its active power generated from the converter and regulate the voltage magnitude at PCC by governing the delivered reactive power. As the control objective of Grid-Forming Converters (GFMs) is to stabilise the terminal voltage rather than directly controlling the currents, a significant increase of currents could occur during faults. To safeguard the converter operation during the fault, a proper FRT strategy should be designed to limit the current magnitude, while maintaining the injection of reactive currents to support the system voltage.

Distance protection is one of the main protection schemes widely used in transmission networks around the world. Different from Synchronous Generation (SG), the fault characteristics of CBRs are mainly governed by their embedded controllers. The design of the controller is affected by the associated grid codes and current limiting strategy [10]. Recent research work has found that the massive integration of CBRs can present significant challenges to the reliable operation of distance protection [11][12][14]. In [11], it was found that the connection of CBRs in the network could increase the angle difference between the current infeed from the local and remote ends of the protected line, thus leading to over/under reach issues. The impact of different converter control modes on the performance of distance relay is analysed in [12]. Based on the results, when the CBRs operate in the constant reactive power control mode [13], the distance relays will suffer from the impedance measurement issues, potentially leading to protection failure, especially in the event of phase-to-phase faults. The issues discussed in [11][12] are also observed in [14], where a Hardware-in-the-Loop (HiL) platform is developed to test a physical relay's performance. Furthermore, in [14], it is also found that the integration of an HVDC system can result in an abnormal increase of the

healthy phase current, which will subsequently lead to the faulty phase selection failure in distance protection. However, in the existing research activities, all of the converters under investigation operate in the grid-following mode, and the impact of GFMs on the distance protection have not been investigated comprehensively. GFMs, which have gained significant interests in recent years and are expected to play a major role in future network, could have very different FRT strategies from GFLs. Therefore, it is critical to understand how the integration of GFMs and their different FRT methods could affect distance protection operation.

In this paper, the fundamentals of the GFMs and the typical FRT strategies are reviewed. Case studies of distance protection performance with the fault infeed from a GFM with different FRT strategies are presented. The studies will focus on two main FRT implementations, i.e. the current control-based FRT, and the virtual impedance-based FRT.

The rest of the paper is structured as follows: Section 2 reviews the fundaments of the GFMs and the typically adopted FRT methods; Section 3 discusses the modelling of GFMs with two different FRT strategies; Section 4 presents the test information and the simulation results from RTDS, along with theoretical analysis; the conclusion is provided in Section 5.

2 Fundamentals and FRT Strategies of GFMs

2.1 Fundamentals of GFMs

The network in Fig. 1 is used to illustrate the fundamentals of GFMs, where the active power transmitted between the GFMs and the AC network can be described by (1). In this equation, the V_g and V_{PCC} are the magnitudes of grid-side voltage and the voltage at the PCC; X is the equivalent reactance between the converter and the grid; δ_g and δ_{PCC} are the phasor angles of the grid-side voltage and the voltage at the PCC [15].

$$P = \frac{V_g V_{PCC}}{X} sin(\delta_{PCC} - \delta_g) \quad (1)$$

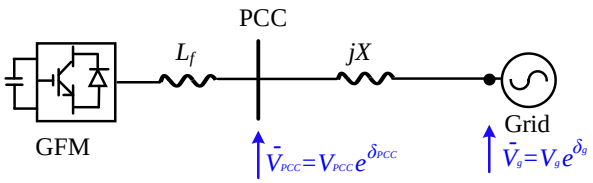

Fig. 1 Typical GFM connection to AC network

In (1), V_g, X, δ_g are dependent on the operating condition of the grid, and their values are considered constant during steady-state operation. With the voltage control loop in the GFM, the V_{PCC} will be kept the same as the voltage reference in the controller by regulating the injected reactive power from the converter, so the V_{PCC} is also constant during steady-state operation. Therefore, (1) establishes the relationship between the active power from the converter and the angle of the voltage phasor at the PCC, which reveals that the angle of voltage at the PCC, δ_{PCC}, could be controlled by regulating the active power from the GFM [15]. As GFMs are capable of synchronising to the grid by themselves without the need for PLLs, GFMs largely mitigate the loss of synchronism risks in weak systems and are capable of operating in a network without SGs. More information about the GFM fundamentals can be found in [15].

2.2 FRT strategies of GFMs

Based on existing literature, the FRT strategies typically used by GFMs can be categorised into four groups, i.e., 1) switching to the grid-following mode (also termed 'current control mode') [16]; 2) introducing the virtual impedance [17][18]; 3) adding a cascade inner current control loop and saturating the current references [19][20]; and 4) readjusting the power references during the faults [21][22].

2.2.1 Current control-based FRT: with the current control-based FRT strategy, GFMs will switch to the grid following mode to limit the fault current and inject the required level of reactive currents based on grid code requirements. In this method, a backup PLL is required to synchronise with the main network during the faults and undesired transients could appear owing to the mode transition between the normal operating mode, i.e., grid-forming, and the fault mode, i.e., grid-following mode. Additionally, the converter behaves as a current source rather than the voltage source during the faults, therefore, this FRT strategy is undesirable for islanded networks fully dominated by the CBRs.

2.2.2 Virtual impedance-based FRT: The virtual impedance-based FRT strategy is realised by adding a virtual impedance inside the converter control loop to achieve the same performance as increasing the converter output impedance, thus limiting the current magnitude of the converter. In this way, the converter can maintain the voltage source behaviour before, during and after faults, therefore, it provides a valuable perspective for the current limitation of GFMs. However, since the virtual impedance cannot abruptly modify the current amplitude, some transients in current during the initial period of fault might appear in the virtual impedance based FRT structure [18].

2.2.3 Current reference saturation-based FRT: The reference saturation-based method is realised by saturating the current references of the additionally introduced inner current controller. However, as suggested in [23], the saturated current references will result in saturation of the voltage regulator, which causes improper alignment of the voltage in the dq frame. Finally, this will lead to the wind-up and the instability issues of the GFM.

2.2.4 Power references readjustment-based FRT: In this FRT strategy, the current magnitude is limited by scaling down the power references of the GFMs. The amounts of injected reactive power during the faults can be controlled by governing the reactive power reference. Comparing to the other aforementioned FRT strategies, the power reference readjustment-based FRT is not frequently used in the GFMs.

3 Modelling of GFM with Different FRT Strategies

In this paper, two FRT strategies with highest potential for practical application, i.e. current control-based FRT and the virtual impedance-based FRT, are adopted for implementing the GFM model in RSCAD (a software package for RTDS), which are used for evaluating the impact of GFMs on distance protection performance.

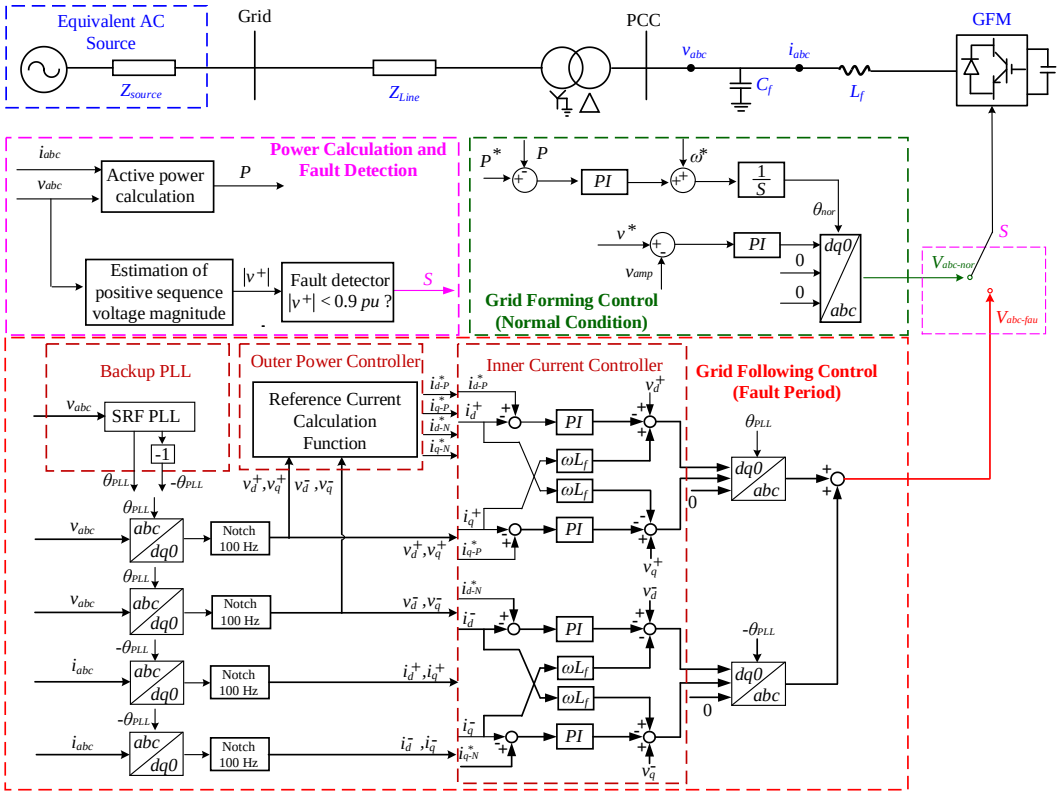

Fig. 2 Current control-based FRT strategy

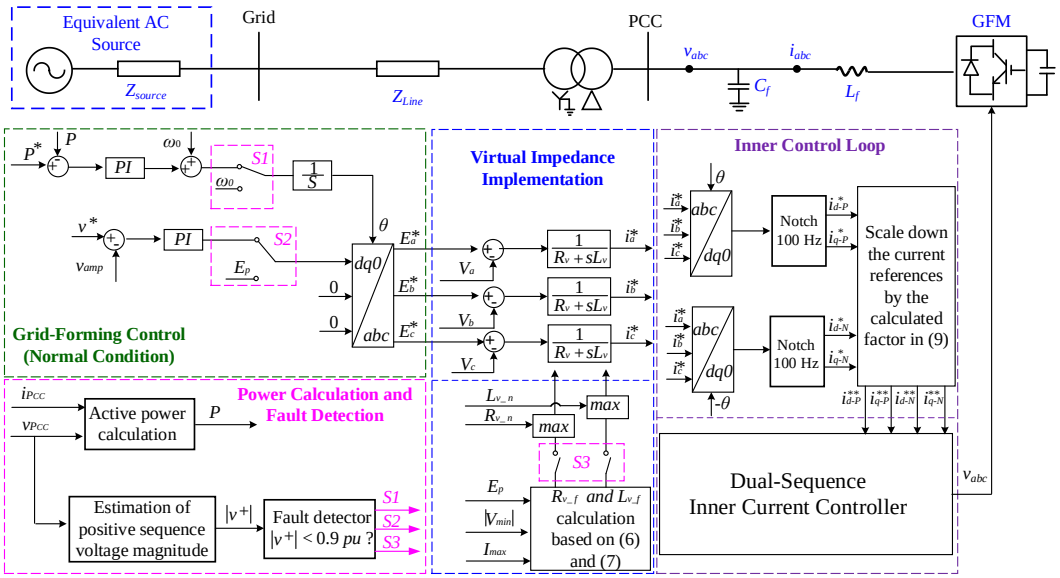

Fig. 3 Virtual impedance-based FRT strategy [18]

3.1 Design and implementation of current control based FRT

The structure of the GFM with current control-based FRT strategy is shown in Fig. 2, where there are three main modules, i.e., power calculation and fault detection module, grid-forming control module for normal condition operation, and grid-following control module for fault conditions. In the power calculation and fault detection module, the magnitude of the positive sequence voltage is measured and compared to the defined voltage threshold to detect the fault. The output signal '*S*' is used to control the switching action of the GFM. In the developed GFM model, the voltage threshold is set as 0.9 pu, which has been chosen empirically and could be adjusted depending on specific system parameters.

During normal conditions, the angle and amplitude of the voltage at the PCC are governed by the grid-forming control by regulating the active and reactive power transmitted to the main grid. When a fault occurs in the network, the controller will be activated to limit the current magnitude and inject the reactive currents to the main system. The current references during the fault period are presented in (2) to (4), following the requirement in the current GB Grid Code [24], where the $|v^+|$ is the magnitude of the positive sequence voltage; i^*_{d-P}, i^*_{q-P}, i^*_{d-N} and i^*_{q-N} are the positive and negative sequence active and reactive current references on the d and q axes.

$$i^*_{q-P}(pu) = -3.28|v^+| + 2.64, 0 \le i^*_{q-P} \le 1 \qquad (2)$$

$$i_{d-P}^{*}\,(pu) = \sqrt{1.2^2 - \left(i_{q-P}^{*}\right)^2} \tag{3}$$

$$i_{d-N}^{*} = i_{q-N}^{*} = 0 \tag{4}$$

3.2 Virtual impedance-based FRT strategy

The structure of the GFM with virtual impedance-based FRT strategy is shown in Fig. 3, which is designed based on [18]. As shown in Fig. 3, in the developed virtual impedance based GFM model, the same modules of the grid-forming control during normal condition and the fault detection are implemented as the module structures presented in Section 3.1. Once the fault is detected, the switch '$S1$' and '$S2$' will connect to the paths with the inputs of ω_0 and E_p and the switch '$S3$' will be closed to introduce the virtual impedance calculated during the fault period.

The equations used to calculate the virtual impedance during faults are presented in (5) to (7) [18], where E_p is the peak value of the phase voltage; $|V_{min}|$ is the minimum amplitude of the voltage at PCC; I_{max} is the maximum tolerable currents of the GFM, i.e., 1.2 pu assumed in this work; XR_{ratio} is the X/R ratio of the introduced virtual impedance and ω_0 is the fundamental angular frequency.

$$Z_{v\_f} = \frac{E_p - |V_{min}|}{I_{max}} \tag{5}$$

$$R_{v\_f} = \frac{Z_{v\_f}}{\sqrt{XR_{ratio}^2 + 1}} \tag{6}$$

$$L_{v\_f} = \frac{\left(XR_{ratio} \cdot R_{v\_f}\right)}{\omega_0} \tag{7}$$

For the measurement of $|V_{min}|$, the two-sample based amplitude estimation technique [25] is implemented to replace the Kalman filter in [18], which largely simplifies the peak estimation structure and decreases the computation burden. The principle of the two-sample based technique is presented in (8), where v_k and v_{k+1} are the k^{th} and $(k+1)^{th}$ samples of the measured three-phase voltage and Δt is the time difference between the samples of v_k and v_{k+1}.

$$|V_{min}|^2 = \frac{v_k^2 + v_{k+1}^2 - 2v_k v_{k+1}\, cos(\omega_0 \Delta t)}{(sin(\omega_0 \Delta t))^2} \tag{8}$$

As mentioned in Section 2.2.2, initial transients could appear as the virtual impedance cannot abruptly modify the current amplitude. Such undesired transients can be dangerous for the actual implementation on the hardware platform, therefore, an additional limiting strategy has been employed in the inner current loop to scale down the current references by the calculated scaling factor in (9), which guarantees the current is always within the required limit.

$$SF = \frac{\sqrt{(i_{d-P}^{*})^2 + \left(i_{q-P}^{*}\right)^2} + \sqrt{(i_{d-N}^{*})^2 + \left(i_{q-N}^{*}\right)^2}}{I_{max}} \tag{9}$$

4 Simulation Results and Analysis

4.1 Test network

The diagram of the network used for the study is shown in Fig. 4, and the associated parameters are presented in Table 1. The performance of the relay at converter side is investigated, with its settings presented in Table 2. Table 3 presents the list of studies that have been conducted, where the capacity of the studied GFM and the fault level of SG1 are maintained at 839 MVA and 3000 MVA respectively. Furthermore, the current magnitudes of GFM in both FRT strategies are restricted to no more than 1.2 pu.

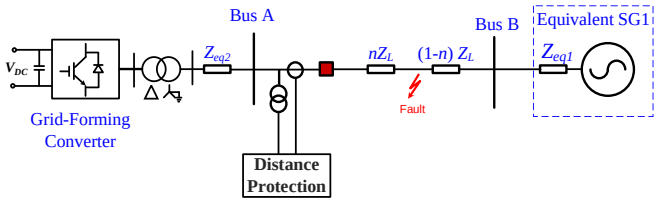

Fig. 4 Schematic of the network investigated in case studies

Table 1 Parameters of the protected line

Parameters	Definition	Values
V_{LL}	Nominal line to line voltage	275 kV
L	Protected line length	12.1 km
r_1 , r_0	Positive and zero sequence resistance per km	r_1=0.0378 Ω/km, r_0=0.159 Ω/km.
l_1 , l_0	Positive and zero sequence inductance per km	l_1=1.324 mH/km, l_0=3.202 mH/km.
c_1 , c_0	Positive and zero sequence capacitance per km	C_1=8.964 nF/km, C_0=6.48 nF/km.

Table 2 Settings of the distance relay model

Parameters	Distance Relay Settings
Characteristic	QUAD
Reach settings	Zone 1: 80 %; Zone 2: 120 %;
Residual compensation factor	$K_0 = 0.48\angle -6.4°$
Time delay	Zone 1: 0 ms; Zone 2: 400 ms;
Right resistive reach	6.72 Ω
Left resistive reach	1.68 Ω
Directional angle	30°
Tilt angle	−3°

Table 3 Information of the studied cases

Cases	FRT Strategy of GFM	Fault Conditions
1	Current control-based	AG, 15%, 2 Ω
2		AB, 15%, 2 Ω
3		ABCG, 15%, 2 Ω
4	Virtual impedance-based	AG, 15%, 2 Ω
5		AB, 15%, 2 Ω
6		ABCG, 15%, 2 Ω

4.2 Simulation results and analysis

For ease of comparison, in the following studies, the RTDS simulation results under the same network conditions will be investigated together, i.e., Case 1 and Case 4, Case 2 and Case 5, Case 3 and Case 6, to evaluate the impact of applying two different FRT strategies on distance protection operation.

4.2.1 Analysis of the distance relay performance in Case 1 and Case 4: The impedance locus measured by the distance relay of Case 1 and Case 4 are plotted in Fig. 5. As shown in Fig. 5, the distance relay should trip as the measured impedance locus moves into zone 1. However, the relay can fail to trip due to the phase selection problem as reported in [14].

In some physical relays, the phase selection function is realised by comparing the magnitudes of superimposed phase-to-phase

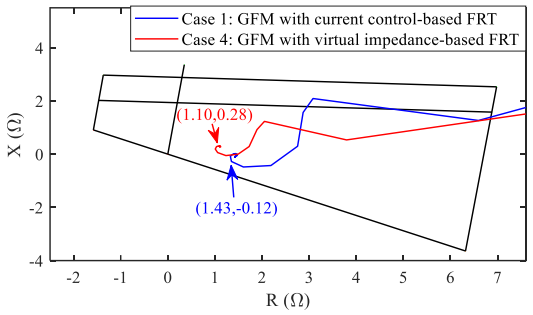

Fig. 5 Impedance locus measured by the distance relay

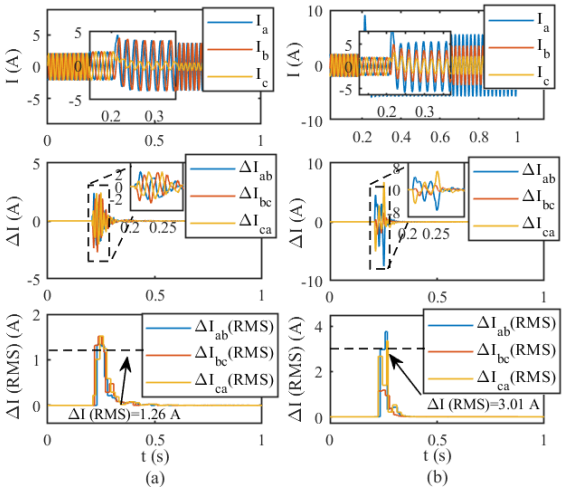

Fig. 6 Input phase currents, superimposed phase to phase currents and the RMS values of phase to phase superimposed currents of relay, (a) Case 1, (b) Case 4.

currents, i.e., ΔI_{ab}, ΔI_{bc} and ΔI_{ca} [26]. Any superimposed currents larger than 80 % of the largest superimposed current are taken into account by the faulty phase selection logic. For the investigated AG fault in Case 1 and Case 4, the relay can detect the faulted phase successfully when the magnitude of ΔI_{ab} and ΔI_{ca} increase to a similar value, while the ΔI_{bc} is lower than the threshold. However, by observing the values of the ΔI (RMS) in Fig. 6 (a), the magnitudes of the three superimposed currents are all greater than the defined threshold in Case 1, i.e., 1.26 A in Fig. 6 (a), which leads to the incorrect phase selection and thus failure in tripping. From Fig. 6 (b), it can be seen that the expected condition of the superimposed currents, i.e., only the magnitudes of ΔI_{ab} and ΔI_{ca} greater than the threshold, is observed when the GFM adopts the virtual impedance-based FRT.

Moreover, by comparing the reactance measured by the distance relay in Fig. 5, the value measured in Case 4 is closer to the assumed reactance of 0.36 Ω. This suggests that the virtual impedance-based FRT strategy is also superior in terms of fault impedance estimation and can mitigate the over-reach issues compared with the current control-based method.

4.2.2 Analysis of the distance relay performance in Case 2 and Case 5: As reported in [11][14], the large angle difference of the current infeed from two ends of the protected line when GFM using the constant current control (case 2) can lead to severe over/under reach issues. As shown in the impedance locus in Fig. 7 (a), when the GFM uses the current control-based FRT, a severe over-reach problem occurs, caused by the large angle displacement between the currents fed from both ends of the line, i.e., $\Delta\psi = -81.81^{\circ}$, which is illustrated in Fig. 7 (b). This results in the measured impedance being on the reverse side of the protective zone, thus resulting in the protection failure. By comparing the values of $\Delta\psi$ in Case 2 and Case 5, it is apparent that the virtual impedance-based FRT strategy provides a much more protection-friendly choice, where the measured impedance is more accurate in reflecting the real fault location, as the angle difference observed between the fault currents from the two ends is much smaller.

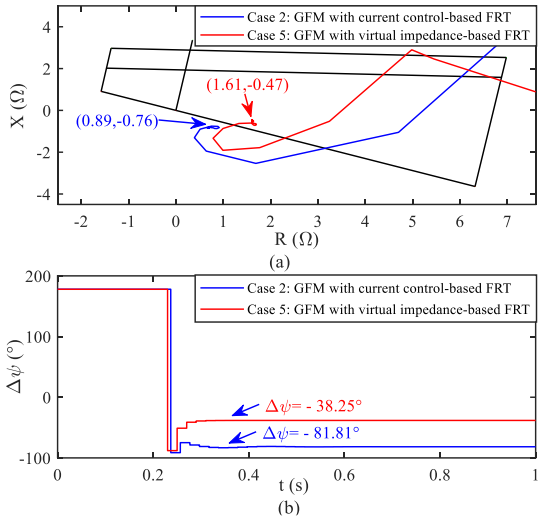

Fig. 7 Simulation results of case 2 and case 5, (a) impedance locus measured by the relay during the AB faults, (b) values of the angle difference of the infeed from both sides of the protected line

4.2.3 Analysis of the distance relay performance in case 3 and case 6: based on the HiL results in [14], the distance relay will trip in zone 2 with the fault on the 15 % of the protected line when the converter operates at the grid-following mode during the faults. The zone discrimination issues are introduced by the oscillation of the measured impedance as shown in Fig. 8 (a). Such undesired oscillation is due to the significant voltage drop in balanced faults, e.g., ABCG fault in Case 3 and 6, the converter controlled by the grid-following mode cannot follow the grid properly owing to the synchronisation issues of the PLL. The tracking issue results in the oscillation of the positive

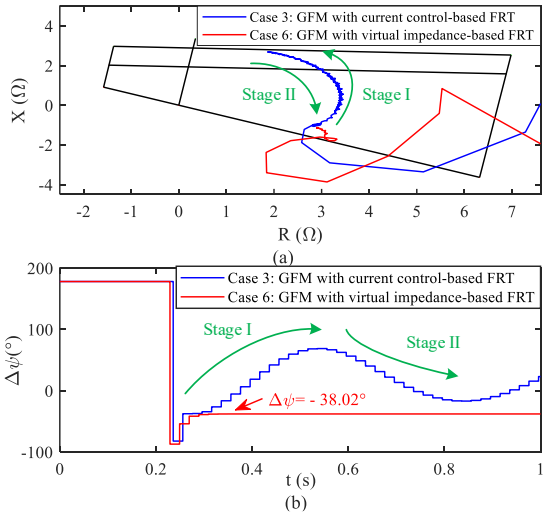

Fig. 8 Simulation results of case 3 and case 6, (a) impedance locus measured by the relay during the ABCG faults, (b) values of the angle difference of the infeed from both sides of the protected line

sequence currents on the dq axes of the converter controller, which causes the angle variation of the current generated from the converter. Finally, the angle variation will be reflected by the impedance measurement of the distance relay through affecting the angle difference of current infeed from both ends of the protected line. However, with the proposed virtual impedance-based GFM, as the PLL does not need to be implemented, the aforementioned oscillating issue has been largely mitigated. This is evident from the results of Case 6 as shown in Fig. 8.

5 Conclusion

In this paper, the impact of GFMs on the distance protection performance has been evaluated. The GFM studied are equipped with two typically adopted FRT methods, i.e. current control-based FRT and virtual impedance-based FRT. For the current control-based approach, the GFM limits the current magnitude and injects the required level of reactive current by regulating the current reference directly. However, after switching to the grid-following mode, the converter will behave as a current source and loose the voltage source behaviour, therefore, it is not suitable for the islanded system with CBRs only. In this case, a backup PLL is usually necessary. To address those issues, the virtual impedance-based FRT strategy was also implemented in this paper and its impact on distance protection performance compared to the current control-based method. According to the simulation results, it was found that the distance protection has overall much better performance when the GFM is equipped with the virtual impedance-based strategy. Additionally, due to the PLL-free structure, the virtual impedance-based method also has a better performance during the balanced fault conditions in injecting required currents, thus can largely mitigate risk of protection failure.

6 References

[1] National Grid ESO, Future Energy Scenarios, 2020.

[2] R. Rosso, X. Wang, M. Liserre, X. Lu and S. Engelken, "Grid-forming converters: an overview of control approaches and future trends," *2020 IEEE Energy Conversion Congress and Exposition (ECCE)*, 2020, pp. 4292-4299.

[3] Q. Hu et al., "Large Signal Synchronizing Instability of PLL-Based VSC Connected to Weak AC Grid," in *IEEE Trans. on Power Systems*, vol. 34, no. 4, pp. 3220-3229, July 2019.

[4] M. Davari and Y. A. I. Mohamed, "Robust Vector Control of a Very Weak-Grid-Connected Voltage-Source Converter Considering the Phase-Locked Loop Dynamics," in *IEEE Trans. on Power Electronics*, vol. 32, no. 2, pp. 977-994, Feb. 2017.

[5] M. Saleem, C. Ki-Young, K. Rae-Young, Resonance damping for an LCL filter type grid-connected inverter with active disturbance rejection control under grid impedance uncertainty, *International Journal of Electrical Power & Energy Systems*, Vol. 109, pp. 444-454, 2019.

[6] F. Alsokhiry, G.P. Adam, Y. Al-Turki, Limitations of voltage source converter in weak ac networks from voltage stability point of view, *International Journal of Electrical Power & Energy Systems*, Vol. 119, 2020.

[7] Y. Huang, X. Yuan, J. Hu, P. Zhou and D. Wang, "DC-Bus Voltage Control Stability Affected by AC-Bus Voltage Control in VSCs Connected to Weak AC Grids," in *IEEE Journal of Emerging and Selected Topics in Power Electronics*, vol. 4, no. 2, pp. 445-458, June 2016.

[8] J. Rocabert, A. Luna, F. Blaabjerg and P. Rodríguez, "Control of Power Converters in AC Microgrids," in *IEEE Transactions on Power Electronics*, vol. 27, no. 11, pp. 4734-4749, Nov. 2012.

[9] S. D'Arco and J. A. Suul, "Equivalence of Virtual Synchronous Machines and Frequency-Droops for Converter-Based MicroGrids," in *IEEE Trans. on Smart Grid*, vol. 5, no. 1, pp. 394-395, Jan. 2014.

[10] A. Hooshyar et al., "Distance protection of lines emanating from full-scale converter-interfaced renewable energy power plants—part i: Problem statement," *IEEE Trans. on Power Delivery*, vol. 30, no. 4, pp. 1770–1780, 2015.

[11] Y. Fang, K. Jia, Z. Yang, Y. Li and T. Bi, "Impact of Inverter-Interfaced Renewable Energy Generators on Distance Protection and an Improved Scheme," in *IEEE Trans. on Industrial Electronics*, vol. 66, no. 9, pp. 7078-7088, Sept. 2019.

[12] J. Jia et al., "Impact of VSC Control Strategies and Incorporation of Synchronous Condensers on Distance Protection Under Unbalanced Faults," in *IEEE Trans. on Industrial Electronics*, vol. 66, no. 2, pp. 1108-1118, Feb. 2019.

[13] P. Rodriguez et al., "Safe current injection strategies for a STATCOM under asymmetrical grid faults," *IEEE Energy Conversion Congress and Exposition*, Atlanta, GA, 2010, pp. 3929-3935.

[14] D. Liu, Q. Hong, A. Dyśko, D. Tzelepis, C. Booth, I. Cowan and B. Ponnalagan, "Hardware-in-the-loop tests and analysis of HVDC system's impact on distance protection performance," in *The 17th International Conference on AC and DC Power Transmission*, Dec. 2021.

[15] A. Monti, F. Milano , E. Bompard and X. Guillaud, Converter-Based Dynamics and Control of Modern Power Systems, 2021.

[16] A. Abdelrahim et al., "New Fault Detection Algorithm for an Improved Dual VSM Control Structure With FRT Capability," in *IEEE Access*, vol. 9, pp. 125134-125150, 2021.

[17] G. Denis et al., "The migrate project: The challenges of operating a transmission grid with only inverter-based generation. A grid-forming control improvement with transient current-limiting control," *IET Renewable Power Gener.*, vol. 12, no. 5, pp. 523–529, Apr. 2018.

[18] R. Rosso et al., "On The Implementation of an FRT Strategy for Grid-Forming Converters Under Symmetrical and Asymmetrical Grid Faults," in *IEEE Trans. on Industry Applications*, vol. 57, no. 5, pp. 4385-4397, Sept.-Oct. 2021.

[19] B. Mahamedi et al., "Sequence-Based Control Strategy With Current Limiting for the Fault Ride-Through of Inverter-Interfaced Distributed Generators," in *IEEE Trans. on Sustainable Energy*, vol. 11, no. 1, pp. 165-174, Jan. 2020.

[20] A. Gkountaras, S. Dieckerhoff and T. Sezi, "Evaluation of current limiting methods for grid forming inverters in medium voltage microgrids," *2015 IEEE Energy Conversion Congress and Exposition (ECCE)*, 2015, pp. 1223-1230.

[21] M. G. Taul et al., "Current Limiting Control With Enhanced Dynamics of Grid-Forming Converters During Fault Conditions," in *IEEE Journal of Emerging and Selected Topics in Power Electronics*, vol. 8, no. 2, pp. 1062-1073, June 2020.

[22] A. Abdelrahim et al., " Modified grid forming converter controller with fault ride through capability without PLL or current loop," in *Proc. 18th Wind Integr. Workshop*, Dublin, Ireland, 2019, pp. 1-8.

[23] A. D. Paquette and D. M. Divan, "Virtual Impedance Current Limiting for Inverters in Microgrids With Synchronous Generators," in *IEEE Transactions on Industry Applications*, vol. 51, no. 2, pp. 1630-1638, March-April 2015.

[24] The Grid Code Issue 5 Revision 21, National Grid, London, UK.

[25] T. Bajanek and J. Orgasova, "Instantaneous and Definite Time Overcurrent Protection Algorithms," in *Proceedings of the 21st Conference STUDENT EEICT*, 2015, pp. 590–594.

[26] Technical Manual: MiCOM, P40 Agile P443 ver92, June 2020.